Lawrence Berkeley National Laboratory
LBL Publications

Title
Visualizing the performance loss of solar cells by IR thermography — an evaluation study on CIGS with artificially induced defects

Permalink
https://escholarship.org/uc/item/9pn813nm

Journal
Progress in Photovoltaics Research and Applications, 24(7)

ISSN
1062-7995

Authors
Vetter, Andreas
Babbe, Finn S
Hofbeck, Bernhard
et al.

Publication Date
2016-07-01

DOI
10.1002/pip.2749

Peer reviewed

eScholarship.org Powered by the California Digital Library
University of California

Progress in PHOTOVOLTAICS

PROGRESS IN PHOTOVOLTAICS: RESEARCH AND APPLICATIONS
Prog. Photovolt: Res. Appl. (2016)
Published online in Wiley Online Library (wileyonlinelibrary.com). DOI: 10.1002/pip.2749

RESEARCH ARTICLE

Visualizing the performance loss of solar cells by IR thermography — an evaluation study on CIGS with artificially induced defects

Andreas Vetter[1]*, Finn S. Babbe[2], Bernhard Hofbeck[1], Peter Kubis[3], Michael Richter[2], Stephan J. Heise[2], Jörg Ohland[2], Ingo Riedel[2] and Christoph J. Brabec[3]

[1] Bavarian Center for Applied Energy Research (ZAE Bayern), Energie Campus Nürnberg, Fürther Str. 250, 90429 Nürnberg, Germany
[2] Laboratory for Chalcogenide Photovoltaics (LCP), Energy and Semiconductor Research Laboratory, Department of Physics, University of Oldenburg, Carl-von-Ossietzky-Strasse 9-11, 26129 Oldenburg, Germany
[3] Institute of Materials for Electronics and Energy Technology (i-MEET), University of Erlangen-Nuremberg, Martensstraße 7, 91058 Erlangen, Germany

ABSTRACT

Local electric defects may result in considerable performance losses in solar cells. Infrared (IR) thermography is one important tool to detect these defects on photovoltaic modules. Qualitative interpretation of IR images has been carried out successfully, but quantitative interpretation has been hampered by the lack of “calibration” defects. The aims of this study are to (i) establish methods to induce well-defined electric defects in thin-film solar cells serving as “calibration” defects and to (ii) assess the accuracy of IR imaging methods by using these artificially induced defects. This approach paves the way for improving quality control methods based on imaging in photovoltaic. We created ohmic defects (“shunts”) by using a focused ion beam and weak diodes (“interface shunts”) by applying a femto-second laser at rather low power on copper indium gallium selenide cells. The defects can be induced precisely and reproducibly, and the severity of the defects on the electrical performance can be well adjusted by focused ion beam/laser parameters. The successive assessment of the IR measurement (ILIT-Voc) revealed that this method can predict the losses in P_{mpp} (maximal power extractable) with a mean error of below 10%. Copyright © 2016 John Wiley & Sons, Ltd.

KEYWORDS
perfomance; imaging; PV modules; defects

***Correspondence**
Andreas Vetter, Bavarian Center for Applied Energy Research (ZAE Bayern), Energie Campus Nürnberg, Fürther Str. 250, 90429 Nürnberg, Germany.
E-mail: vetter@zae.uni-erlangen.de

Received 16 September 2015; Revised 3 December 2015; Accepted 21 December 2015

1. INTRODUCTION

Photovoltaic electric current generation is one of the most important keys for future renewable energy supply. The concept of thin-film solar cells based on copper indium gallium selenide (CIGS) is one promising approach for a further decrease of the price of PV modules. Indeed, significant progress has been achieved in increasing the efficiency up to 21.7% for single cells [1]. The power conversion efficiencies of CIGS modules have reached 18.7% for mini-modules and surpassed 15% for conventional modules easily [2]. One contribution to this discrepancy between cell and module efficiency probably results from laterally spread electric defects that may hinder a further increase in module efficiency. These defects may be either induced during processing or also during outdoor usage.

Different types of defects have been observed and result in a reduction of the module performance [3–8]. From the electrical viewpoint, defects (or shunts) may lead to a local short current. Such defects are classified depending on their electrical behavior as either weak diodes or “classic” shunts (locally reduced parallel resistance). Computer simulations have been applied modeling the electrical network of photovoltaic (PV) modules in order to understand the

Copyright © 2016 John Wiley & Sons, Ltd.

influence of different defects on the performance of the module [9,10]. One theoretical study showed, for example, that defects at different positions on the cell lead to a different influence on module performance [11]. The aim of such studies is to gain a better understanding of the photo-physical processes, which can then pave the way to optimized module efficiency by improving cell architecture. So far, these photo-physical investigations of defects have been studied systematically only by computer models, because in reality, defects occur rather undefined and randomly on PV modules. The possibility of inducing well-defined defects at selected positions on the module or cell would be a highly valuable tool enabling also experimental studies on the photo-physics of solar cells with defects.

Local electric defects creating short currents may be localized by infrared thermography but also by luminescence imaging [12–14]. Locally increased current densities lead to an increase in locally dissipated power, thus resulting in a hot spot visible by infrared (IR) cameras. This technique has been proven to be an ideal tool for electrical defect characterization, especially when applying highly sensitive IR cameras and in combination with a pulsed excitation with lock-in analysis. In doing so, even small defects resulting in very low temperature changes may be detected [15]. This technique is called illuminated lock-in thermography (ILIT) when applying pulsed light for excitation or dark lock-in thermography (DLIT) when applying a pulsed electric current for excitation of the PV module. In addition to the identification of local defects, IR thermography has also been used for material analysis such as determining the local series resistance [16,17]. A further benefit of this imaging method is its speed that qualifies in particular ILIT for an online-quality control [18] as no contacting of the modules is required.

One limitation of experimental defect studies up to now has been that a validation of the results obtained by imaging is hardly possible. This is because defects occur rather randomly on the modules, and their influence cannot be electrically measured or at least varied. Accordingly, a systematic investigation of defects and their influence on the electrical parameters is very difficult. This, in turn, has hampered an assessment of the accuracy of the interpretation of imaging methods regarding electrical parameters. The two aims of this study are to overcome this shortage by (i) establishing methods for inducing well-defined defects with a focused ion beam (FIB) in a scanning electron microscope (SEM) and with a femtosecond (fs) laser and by (ii) assessing the accuracy of ILIT as a contactless tool to predict the losses in performance due to these defects.

2. EXPERIMENTAL PART

In this study, thin-film solar cells based on CIGS samples (processed by co-evaporation) were investigated. The substrate is a 3 mm thick soda-lime-silicate glass covered with a molybdenum back contact. On top of the CIGS absorber, a CdS buffer is deposited followed by ZnO and ZnO:Al as transparent front electrode (TCO). The thickness of the layers altogether is about 3 μm. For further information about the processing, the reader is referred to reference [19]. The samples were not encapsulated, which provided us direct access to the active layers for defect treatment. Only cells without "natural" shunts (as identified by ILIT) were used for the further preparation of artificial shunts.

The samples had a cell width of 4 mm. The cells were connected in series via three patterning lines [19]: P1 separating the back electrode of each cell, P2 realizing the connection of two neighboring cells, and P3 separating the front electrode/active layer of each cell. Two different preparations were carried out: For laser treatment, cell stripes with 4 mm width and 3 cm length were prepared from modules without every other P3 scribe to contact the cell via the TCO of the neighboring cells. Electrical defects were induced with a Nd:YVO4 femtosecond laser (operating at the second harmonic, 520 nm). The repetition rate was 500 kHz, the laser fluence 0.0995 J/cm^2. The overlap of single shots was 90% with an effective beam diameter of 32 +/− 2 μm (diameter of beam @ 1/e2 of maximal energy). Defects were typically created as circles with a diameter of 400 μm.

For the FIB treatment, smaller cells with about 5 mm length were prepared from standard modules with contacting the molybdenum on one adjacent cell and the TCO on the other. A FEI Helios Nanolab SEM with a focused gallium-ion beam was used to create holes with different diameters that reached from the top to the molybdenum back contact. A thin platinum layer was deposited on top of the TCO where the hole was milled to avoid slurred rims from molten ZnO. In total, 20 shunt-free cells were prepared for laser treatment and 18 cells for FIB treatment.

For characterization of the laser-induced defects, a triggerable IR camera (Equus 327 k, IRcam GmbH, Germany) was used. The camera is sensitive in the mid-infrared range (2–5 μm) with a Stirling cooled focal plane array. For ILIT measurements, the excitation of the solar cells was carried out by white LED illumination at low light illumination. The lock-in frequency of the ILIT measurements was 1 Hz. The FIB-treated cells were investigated with an ILIT system from Thermosensorik with 10 Hz lock-in frequency and 1000 W/cm^2 illumination by several arrays of red and blue LEDs.

A scalar parameter, IR_{Signal}, was calculated from the ILIT images in order to determine the electrical losses of the solar cells because of the induced defects via contactless imaging. First, the pixels comprising the defect were defined (by marking these pixels manually by an image processing software, ImageJ). Then, the mean value $I_{healthy}$ of the "healthy" (unharmed) part of the solar cell (excluding the defect area) was calculated. Then, a new image I_1 was calculated by subtracting this mean value from the initial raw image I_0 (Equation (1)). A second post-processed image I_2 was calculated by setting all negative pixel of *I1* to zero. Accordingly, the defect signal could be calculated simply as the sum of the pixels in the area marked as defect.

DOI: 10.1002/pip

The steps are summarized in Equations 1 to 3 (with $I(i,j)$ referring to the local intensity of the according image).

$$I_1(i,j) = I_0(i,j) - I_{healthy} \tag{1}$$

$$I_2(i,j) = \begin{cases} I_1(i,j) & if \ \ I_1(i,j) > 0 \\ 0 & else \end{cases} \tag{2}$$

$$IR_{Signal} = \sum_{k \in Defect} I_2(k) \tag{3}$$

3. RESULTS

3.1. Inducing "classic" shunts by focused ion beam

Before investigating the electrical influence of FIB-induced defects, we tested the defect induction on two CIGS samples (1 × 1 cm) without patterning lines. The deposition of a platinum layer on top of the TCO prior to FIB treatment was found to be essential for successfully inducing reproducible defects (data not shown). We treated 49 spots of the samples with the aim to induce the defects in a rectangular grid (5.6 × 5.8 mm) with an ion beam current $I = 40$ pA. All 49 defects (1 μm in diameter) can be easily identified in the ILIT image (Figure 1a), which means all defects were induced successfully. The according analysis of the intensity of the defects as observed by the ILIT image is shown in Figure 1b. A slight decreasing trend in the signal intensity with higher spot number is visible, which could be caused by a slightly inhomogeneous illumination. The mean IR signal amplitude of the defects is 79.7 mK (±10.1 mK). On a second sample, we induced the same defect pattern with $I = 230$ pA. Again, all defects were induced successfully as confirmed by ILIT. The mean amplitude signal of these defects was found to be 288.5 mK (±41.6 mK).

In the following, we prepared defects on new samples with $I = 230$ pA as higher ILIT amplitudes signify a larger influence of the induced defects on the electrical performance. We prepared 18 single cells and induced one defect each with a diameter of either 1 μm (12 samples) or 2 μm (6 samples). The influence of the defects on the cell performance is shown in Table I. Clearly, larger defects have a more detrimental influence on the electrical performance. The average loss in V_{oc} (open circuit voltage) is almost 10% because of defects with 2 μm diameter, while the loss in P_{mpp} (maximally extractable power of the cell at optimum external load) is more than 60%. The variation of the influence of the induced defects increases with the defect diameter.

We conducted DLIT measurements in order to determine the type of defect induced. Only the IR signal of the defect area is analyzed. By applying forward and reverse voltage, we can clearly see that the induced defects are of ohmic nature (Figure 2).

Scanning electron microscope (SEM) investigations reveal more details of the induced defects. Figure 3a shows a top view SEM image of a FIB-induced defect. SEM cross sections (Figure 3b) indicate that this may be either because of molten Mo that covers the walls of the milled hole and thus electrically connects front and back electrodes of the cell, or a modification of the CIGS at the rim in a way that the chalcopyrite is transformed to a Se-poor or even metallic phase. An increase in conductivity due to gallium ions from the ion beam seems unlikely, because the shunt only appears when the hole is milled down to the Mo layer; perforating the heterojunction is not sufficient to create a shunt (data not shown).

3.2. Inducing weak diodes by femtosecond laser

On each of the samples, we sequentially induced three defects with the fs laser. All defects were placed in the middle of the cell equidistant to the patterning lines (perpendicular to the patterning lines; direction a). The first defect was placed in the middle of the cell along the patterning lines (direction b), then the second defect was placed in the middle between the first defect and the end of the cell (in

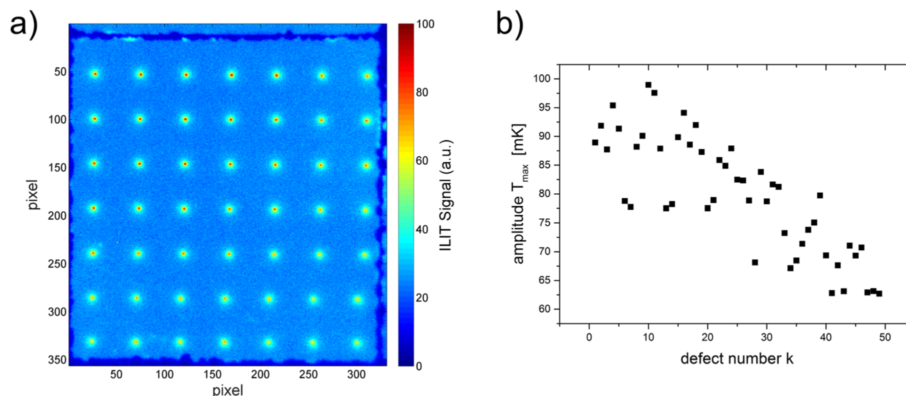

Figure 1. (a) Illuminated lock-in thermography image (10 Hz, 3 min measurement time, 1000 W/m^2 illumination) of sample with defects induced by focused ion beam. (b) Amplitude of the illuminated lock-in thermography signal of each defect.

DOI: 10.1002/pip

Table I. Influence of defect diameter (focused ion beam induced) on the electrical performance. Std. denotes the relative standard deviation; N_s denotes the number of samples.

Diameter defect [μm]	V_{oc} [mV]	Std. [%]	J_{sc} [mA/cm^2]	Std. [%]	P_{mpp}[mW/cm^2]	Std. [%]	N_s
0	698.6	0.87	33.3	1.97	16.3	2.81	18
1	670.3	1.12	31.8	2.05	9.93	8.18	12
2	638.4	2.98	30.5	3.09	6.28	16.53	6

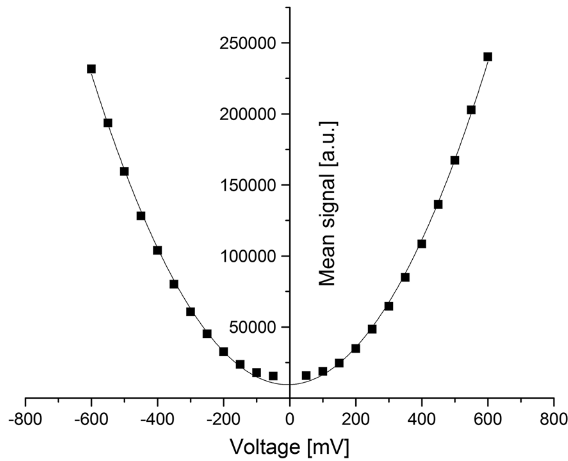

Figure 2. Dark lock-in thermography sweep of focused ion beam-induced defects (infrared signal of the defect on *y*-axis). The defects are characterized as ohmic defects ("classic" shunts) [25].

direction b). The third defect was finally placed in the middle between the first defect and the other end of the cell (in direction b) resulting in a symmetric distribution of the defects. The electrical parameters of the cells depending on the number of defects are listed in Table II. The standard deviations of V_{oc} and J_{sc} are rather low for defect-free cells (1.36% or 1.15%, respectively), while the values for P_{mpp} obviously show a larger variation. The short circuit current (J_{sc}) does not vary with increasing number of defects as the active area of the cells was hardly decreased by the laser-induced defects. The standard deviations of the parameters do not or only slightly increase when inducing defects (Table II). This means that the influence of each induced defect is comparable for all investigated samples. Accordingly, the method to induce defects shows good reproducibility.

Again, we applied DLIT to determine the type of the induced defect. In forward direction (positive voltage), the IR image displays one hot spot for each defect (similar to the results for FIB-induced defects). The actual shape of the defects cannot be seen in the IR image because of heat conduction (resulting in a blurring of the temperature distribution). Results for an exemplary sample with one defect are given in Figure 4. With increasing voltage, an exponential increase in the DLIT signal over the defect is observed (forward bias). Only a very minor increase in the DLIT signal is observed under reverse bias (meaning only a little reduced parallel resistance). The data show that the fs laser-induced defects are weak diodes (with a very slightly reduced parallel resistance).

After inducing the defects, we investigated the surface topology with atomic force microscopy (Figure 5a) and confocal microscopy (data not shown). Both measurements reveal a local surface lift off. The lift off has the same geometry as the laser pattern (circular ring). The height of the material lift off is about 600 nm. At the top of the absorber layer, the transparent conductive electrode is deposited. The interaction of the laser beam and the absorber material results in material sublimation, which subsequently causes the lift off of the transparent electrode. This hypothesis is also confirmed by SEM investigations (Figure 5b and c).

Our results fit well to an approach to pattern CIGS modules by micro-welding using a comparable fs laser reported

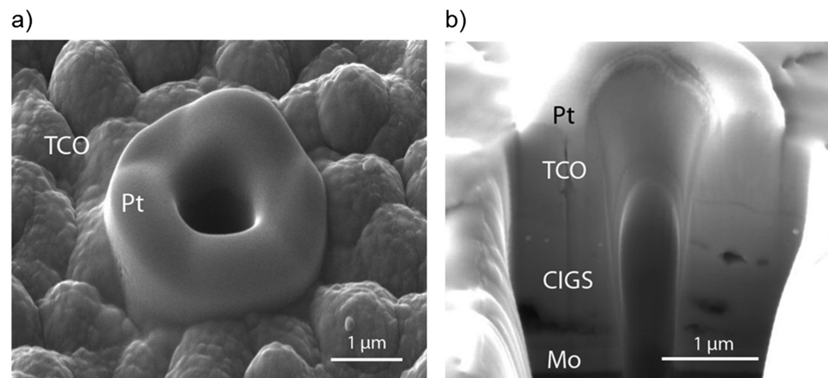

Figure 3. (a) Scanning electron microscope image of a focused ion beam-induced (ohmic) defect, top view. (b) Scanning electron microscope cross section.

Table II. Influence of number of defects (# def.; weak diodes) on the electrical performance. Std. denotes the relative standard deviation; N_s denotes the number of samples.

# def.	V_{oc} [mV]	Std. [%]	J_{sc} [mA/cm2]	Std. [%]	P_{mpp}[mW/cm^2]	Std. [%]	N_s
0	544.8	1.36	0.439	1.15	0.160	5.10	20
1	530.8	1.47	0.429	1.22	0.134	5.28	20
2	515.4	1.71	0.435	1.17	0.124	4.55	19
3	506.7	1.78	0.436	1.22	0.118	3.76	18

Two samples were accidentally broken during undertaking the experiments and were excluded from further analysis. The performance was measured under low light conditions.

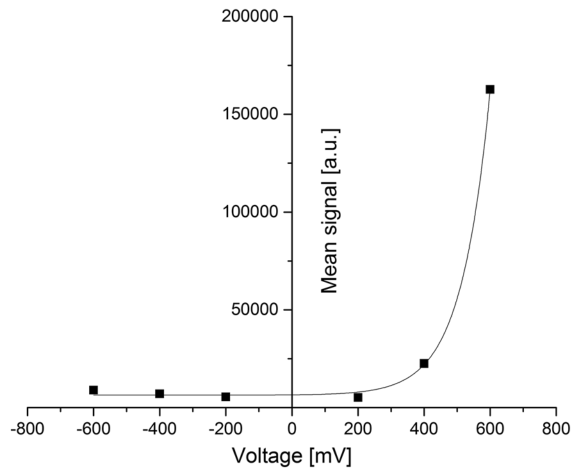

Figure 4. Illuminated lock-in thermography sweep of laser-induced defects (infrared signal of the defect on *y*-axis). The defects are characterized as weak diodes [25].

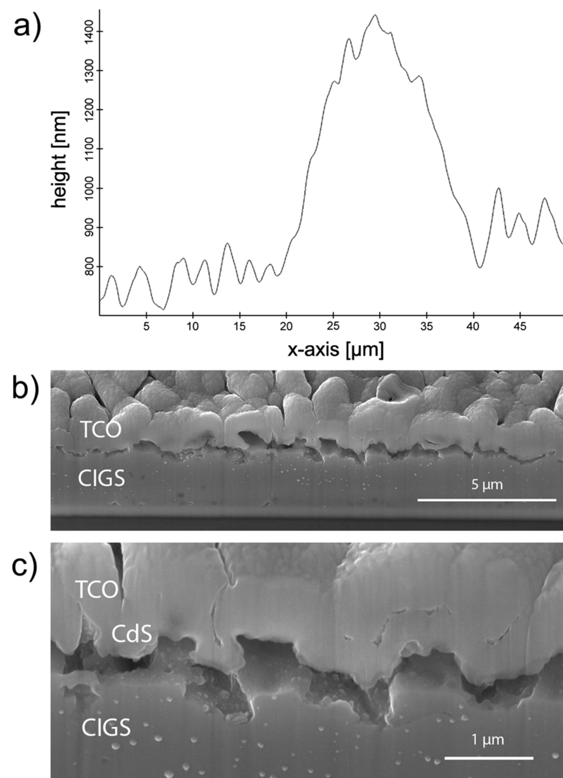

Figure 5. (a) Topology of laser-induced defect via atomic force microscopy scan. (b) Scanning electron microscope cross section of laser-induced defect. (c) Overview on the top, close up below.

in literature [20]. The authors found that adjusting the laser parameters correctly will partly remove the CIGS and create some well around this patterning line (P2). In combination with a change in composition of the CIGS due to the laser treatment, this might serve as electrical contact between front and back contact (P2 line). The authors found the according laser parameters to be around 0.8 W at a repetition rate of 80 kHz [21], which leads to larger energy deposition in CIGS compared with our study (our laser parameters were 0.2 W at a repetition rate of 500 kHz). Accordingly, our results show just some “tiny” TCO lift off. Also, a material variation in the CIGS layer (creating a recombination center) because of the laser beam is likely, in particular close to the front contact.

3.3. Assessment of the illuminated lock-in thermography accuracy on predicting losses in performance

Finally, we considered the question whether the losses in the electric performance, quantified by P_{mpp}, may be assessed accurately by IR imaging (ILIT-Voc in our case). Accordingly, we were looking for a correlation between an IR parameter derived from an ILIT image and the P_{mpp} determined by measuring the JV curve. As previously described (Equations 1–3), one way to quantify the influence of a defect is to calculate a measure (IR_{Signal}) of the shunt intensity compared with the background or “healthy” cell intensity (non-defect area) [15,18]. The larger this value, the larger is the deviation compared with a defect-free cell (with higher P_{mpp}).

Regarding the FIB-treated samples, the losses due to the defects are up to about 60% of the initial P_{mpp} (for 2 µm defects). Figure 6a depicts the IR parameter as a function of the performance loss. A clear correlation between IR_{Signal} and losses in P_{mpp} is found (in our case a linear fit with R^2 of 0.897). The mean absolute deviation of the linear fit and the experimentally derived P_{mpp} was 7.2% (compared with the mean loss due to the shunts). The dynamic

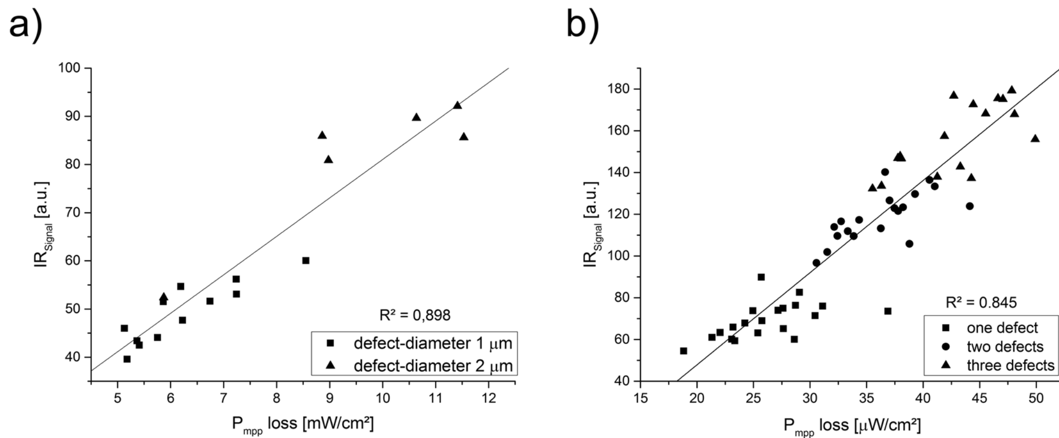

Figure 6. Correlation of infrared signal and loss in P_{mpp}: (a) for focused ion beam-induced defects (ohmic) under one sun illumination and (b) for laser-induced defects (weak diodes) under low light illumination.

range of IR_{Signal} was also found to be good (a factor of 2 between the smallest and the largest signal). Regarding the laser-treated samples (Figure 6b), the losses due to the defects are up to ca. 25% of the initial P_{mpp} when inducing three defects. Again, a clear correlation between the IR signal and losses in P_{mpp} is found (in our case a linear fit with R^2 of 0.845). The mean absolute deviation of the fit to the experimental data was 6.8%. The dynamic range was found to be almost a factor of 5.

4. CONCLUSIONS

Quantitative assessment of IR-shunt-imaging is hardly possible without well-defined defects. In this study, we identified two ways to induce two types of defects in CIGS solar cells. Ohmic defects ("classic" shunts) can be induced by FIB treatment, while an fs laser operated at relatively low power can be used to induce well-defined weak diodes. Both methods have been found to serve as reliable tools to induce defects at a desired location on the cell. Basically, each try to induce a defect was successful after adjusting the settings of FIB and fs laser to our samples. The losses in performance can be easily adapted in a wide range (in this study up to 60% loss in P_{mpp}) by choosing the defect type, changing the size (diameter) of the defect and by the number of the defects induced into the cells. Also, we found that the severity of the created ohmic defects may be adapted by adjusting the ion beam current (FIB), and weak diodes can be adjusted by varying the laser power (data not shown). We used CIGS cells for our study as proof of principle. However, the method is rather easily transferred to other thin-film technologies. The parameters of FIB and fs laser need to be adjusted according to the active layers in this case. One crucial factor to be considered, for example, is the absorptivity of the active layer when treating the sample with a fs laser.

As next step, these tools of creating well-defined defects at selected positions on the cells should be applied to mini-modules. By this, researchers are given the possibility to experimentally study photo-physical phenomena such as the influence of shunt position and the effect of shunt cross talk (interference of defects relatively close to each other) under controlled conditions. The experimental results can also be used to confirm and verify theoretical simulations, which for instance have been published recently [10,11]. A deeper understanding of photo-physical loss mechanisms will support efforts to optimize processing and cell architecture in order to prevent significant losses in the performance of modules due to defects.

Creating well-defined defects opens an exciting opportunity to assess imaging methods. These methods aim at correlating parameters derived by one or several images with electrical parameters of solar cells. Imaging methods are certainly established as *qualitative* tools and have been proven to be valuable tools to gain information on the homogeneity of the material and the number or the types of defects occurring in solar cells. *Quantitative* analyses of imaging techniques have been proposed, but only few efforts on validation of these methods have been spent. This is because module defects typically occur rather randomly, and in general, it is not possible to electrically measure the influence of a single defect on the performance of a cell or a module. A possible, but not elegant, way out of this problem would be to test a large amount of similar (regarding processing conditions) samples and run a statistical analysis. Inducing defects in defect-free cells or mini-modules or adding defects in test modules provides a much more controlled and convenient option to measure the actual influence of specific defects on the electrical performance. This finally enables us to assess the accuracy of predicting the influence of defects by means of imaging methods. An interesting, similar approach has been conducted for photoluminescence imaging on silicon wafers by providing an external short current pathway by Augarten and coworkers [22]. Another approach using DLIT to map the local efficiency of solar cells [23] was recently underpinned by results obtained by computer simulations [24]. In our

study, we aimed at assessing the accuracy of predicting the influence of defects on solar cells by IR measurements (ILIT-Voc). The accuracy was found to be excellent for a wide range of performance loss (from about 10% loss in P_{mpp} caused by weak diodes up to 60% in P_{mpp} caused by ohmic shunts). The mean error in determining the loss in P_{mpp} by ILIT-Voc was significantly below 10%. No optimization of the measurement setup or analysis method has been carried out yet to even further improve this accuracy. Furthermore, we want to point out that the results stem from two different experimental setups indicating the broad applicability of the approach. These results strongly promote ILIT as a reliable, fast and contactless technique for characterization of defects in solar cells. Nevertheless, this proof was carried out for single cells only, and future studies are required to quantify the accuracy of the ILIT-Voc measurements on test modules as well as industrial-scale modules.

ACKNOWLEDGEMENTS

We acknowledge the German Ministry of Economy and Energy for funding (OptiCIGS, 0325724C) and R. Schaeffler and J. P. Theisen (MANZ AG, Germany) for providing the solar cell samples. Andreas Vetter received funding from the “Bavaria on the move initiative” (Energie Campus Nürnberg) by the State of Bavaria. F. S. Babbe, M. Richter, S. J. Heise, and J. Ohland gratefully acknowledge financial support by the EWE AG, Oldenburg, Germany.

REFERENCES

1. Jackson P, Hariskos D, Wuerz R, Kiowski O, Bauer A, Friedlmeier TM, Powalla M. Properties of Cu(In,Ga) Se2 solar cells with new record efficiencies up to 21.7%. *Physica status solidi – Rapid Research Letter* 2015; **9**(1): 28–31.
2. Green MA, Emery K, Hishikawa Y, Warta W, Dunlop ED. Solar cell efficiency tables (Version 45). *Progress in Photovoltaics: Research and Applications* 2015; **23** (1): 1–9.
3. Langenkamp M, Breitenstein O. Classification of shunting mechanisms in crystalline silicon solar cells. *Solar Energy Materials & Solar Cells* 2002; **72**(1–4): 433–440.
4. Breitenstein O, Rakotoniaina JP, Al Rifai MH, Werner M. Shunt types in crystalline silicon solar cells. *Progress in Photovoltaics* 2004; **12**(7): 529–538.
5. Straube H, Wagner J-M, Schneider J, Breitenstein O. Quantitative evaluation of loss mechanisms in thin film solar cells using lock-in thermography. *Journal of Applied Physics* 2011; **110**(8): 084513.
6. Adams J, Vetter A, Hoga F, Fecher F, Theisen JP, Brabec CJ, Buerhop-lutz C. The influence of defects on the cellular open circuit voltage in CuInGaSe 2 thin fi lm solar modules — an illuminated lock-in thermography study. *Solar Energy Materials & Solar Cells* 2014; **123**: 159–165.
7. Buerhop C, Schlegel D, Niess M, Vodermayer C, Weißmann R, Brabec CJ. Reliability of IR-imaging of PV-plants under operating conditions. *Solar Energy Materials & Solar Cells* 2012; **107**: 154–164.
8. Ramspeck K, Bothe K, Schmidt J, Brendel R. Correlation between spatially resolved solar cell efficiency and carrier lifetime of multicrystalline silicon. *Journal Materials Science: Materials in Electronics* 2008; **19** (1): S4–S8.
9. Koishiyev GT, Sites JR. Impact of sheet resistance on 2-D modeling of thin-film solar cells. *Solar Energy Materials & Solar Cells* 2009; **93**(3): 350–354.
10. Malm U, Edoff M. Simulating material inhomogeneities and defects in CIGS thin-film solar cells. *Progress in Photovoltaics* 2009; **17**(5): 306–314.
11. Fecher FW, Romero AP, Brabec CJ, Buerhop-Lutz C. Influence of a shunt on the electrical behavior in thin film photovoltaic modules - A 2D finite element simulation study. *Solar Energy* 2014; **105**: 494–504.
12. Otwin Breitenstein WW, Bauer J, Bothe K, Hinken D, Müller J, Kwapil W, Schubert MC. Can luminescence imaging replace lock-in thermography on solar cells? *IEEE Journal of Photovoltaics* 2011; **1**(2): 159–167.
13. Johnston S, Repins I, Call N, Sundaramoorthy R, Jones KM, To B. Applications of imaging techniques to Si, Cu(In,Ga)Se < inf > 2</inf>, and CdTe and correlation to solar cell parameters. *2010 35th IEEE Photovolt. Spec. Conf.*, pp. 001727–001732, 2010.
14. Hallam B, Augarten Y, Tjahjono B, Trupke T, Wenham S. Photoluminescence imaging for determining the spatially resolved implied open circuit voltage of silicon solar cells. *Journal of Applied Physics* 2014; **115**(4): 044901.
15. Breitenstein O, Warta W, Langenkamp M. *Lock-in Thermography, Basics and Use for Evaluating Electronic Devices and Materials*, 2nd edn. Springer: Berlin, 2010.
16. Breitenstein O, Rakotoniaina JP, van der Heide aSH, Carstensen J. Series resistance imaging in solar cells by lock-in thermography. *Progress in Photovoltaics: Research and Applications* 2005; **13**(8): 645–660.
17. Isenberg J, van der Heide ASH, Warta W. Investigation of series resistance losses by illuminated lock-in thermography. *Progress in Photovoltaics: Research and Applications* 2005; **13**(8): 697–703.
18. Vetter A, Fecher F, Adams J, Schaeffler R, Theisen J-P, Brabec CJ, Buerhop C. Lock-in thermography as a

tool for quality control of photovoltaic modules. *Energy Science & Engineering* 2013; **1**(1): 12–17.
19. Powalla M, Cemernjak M, Eberhardt J, Kessler F, Kniese R, Mohring HD, Dimmler B. Large-area CIGS modules: pilot line production and new developments. *Solar Energy Materials & Solar Cells* 2006; **90**(18–19): 3158–3164.
20. Westin P-O, Zimmermann U, Ruth M, Edoff M. Next generation interconnective laser patterning of CIGS thin film modules. *Solar Energy Materials & Solar Cells* 2011; **95**(4): 1062–1068.
21. Westin P-O, Watjen JT, Zimmermann U, Edoff M. Microanalysis of laser micro-welded interconnections in CIGS PV modules. *Solar Energy Materials & Solar Cells* 2012; **98**: 172–178.
22. Augarten Y, Trupke T, Lenio M, Bauer J, Weber JW, Juhl M, Kasemann M, Breitenstein O. Calculation of quantitative shunt values using photoluminescence imaging. no. March 2012, pp. 933–941, 2013.
23. Breitenstein O. Local efficiency analysis of solar cells based on lock-in thermography. *Solar Energy Materials & Solar Cells* 2012; **107**: 381–389.
24. Breitenstein O, Bauer J, Hinken D, Bothe K. The reliability of thermography- and luminescence-based series resistance and saturation current density imaging. *Solar Energy Materials & Solar Cells* 2015; **137**: 50–60.
25. Bauer J, Breitenstein O, Wagner J-M. Lock-in thermography: a versatile tool for failure analysis of solar cells. *EDFAAO (ASM International)* 2009; **3**: 6–12.